Phase Transitions in Quasi-one-dimensional Selenide BaNbSe$_3$ and Superconductivity in BaNb$_2$Se$_5$

T. Ohtani,[1] S. Honji, and M. Takano*

*Laboratory for Solid State Chemistry, Okayama University of Science, Ridai-cho 1-1, Okayama 700, Japan; and *Institute for Chemical Research, Kyoto University, Uji, Kyoto 611, Japan*

Samples with various compositions around BaNbSe$_3$ were prepared. X-ray analysis revealed that the compound is stable at the composition of BaNb$_{0.80}$Se$_3$, which formally requires Nb^{5+} ions (d^0). The single-phase region extends to the composition BaNb$_{0.95}$Se$_3$. A semiconductor-to-metal transition was observed at ~140 K in BaNb$_{0.95}$Se$_3$. Seebeck measurements showed that the dominant carriers were electrons, which are considered to originate from Nb^{4+} ions (d^1) coexisting with Nb^{5+} ions. On the basis of detailed phase study, the transition was revealed to be intrinsic to BaNb$_{0.95}$Se$_3$ with a very slight Ba deficiency. BaNb$_{0.95}$Se$_3$ with a slight Ba excess shows a semiconductor-to-semiconductor transition at 200–300 K. Seebeck measurements showed that the dominant carriers are electrons above the transition and are holes below the transition. A new compound, BaNb$_2$Se$_5$ with a BaTa$_2$S$_5$-type structure, was found to show superconductivity at 2.5 K. © 1997 Academic Press

INTRODUCTION

Quasi-one-dimensional inorganic compounds show many interesting physical properties associated with their charge density wave (CDW) and spin density wave (SDW) phenomena which originate from strong electron–phonon interactions (1). Many transition metal chalcogenides with quasi-one-dimensional structures were found to exhibit a large variety of phase transitions, e.g., niobium chalcogenides of NbSe$_3$ (2, 3), (NbSe$_4$)$_{10/3}$I (2, 3), Nb$_3$Te$_4$ (4, 5), In$_x$Nb$_3$Te$_4$ (6), and A_xNb$_6$Te$_8$ (A = Tl, La, Nd, etc.) (7) show CDW transitions, and copper sulfides of ACu$_7$S$_4$ (A = Tl, K, Rb) (8, 9) and K$_3$Cu$_8$S$_6$ (10–12) exhibit successive phase transitions possibly including CDW transitions.

Chalcogenides of the general formula BaMX_3 (M = Ti, V, Nb, Ta; X = S, Se) have been found to have a hexagonal BaVS$_3$-type structure with a space group of $P6_3/mmc$ (13–18). A schematic drawing of the structure is shown in

Fig. 1. The structure consists of linear chains of M atoms surrounded by face-sharing chalcogen octahedra, running parallel to the hexagonal c axis. Barium ions separate the chains to enhance the one-dimensionality. Takano *et al.* found that BaVS$_3$ undergoes a phase transition from hexagonal to orthorhombic at 258 K, and exhibits a metal-to-semiconductor (M–S) transition at ~70 K (19, 20). Similar results were reported by Massenet *et al.* (21). Recently, photoemission spectroscopic studies revealed that conduction electrons in BaVS$_3$ behave as a Luttinger liquid (22).

Yan *et al.* found that the stoichiometric BaNbS$_3$ shows metallic behavior, while the sulfur-deficient BaNbS$_{3-\delta}$ ($\delta \approx 0.11$) exhibits a semiconductor-to-metal (S–M) transition at 130 K, accompanied by a structural transition (23). Kim *et al.* found a similar anomaly at ~220 K in the stoichiometric BaNbS$_3$ which they attributed to the coexistence of semiconductive BaNb$_{0.8}$S$_{1-\delta}$ and metallic BaNb$_2$S$_5$ (24). Recently we found similar transitions in electrical resistivity measurements in BaMSe$_3$ (M = Ta, Nb) (25). The temperature variations of the resistivity were observed to be very sensitive to the composition. We speculate, thus, that the discrepancies in the temperature dependencies of the resistivity of BaNbS$_3$ between Yan *et al.* (23) and Kim *et al.* (24) may originate from the difficulty of controlling the compositions. In the present work, we performed the extensive phase study on the BaNbSe$_3$ phase, and investigated the phase transitions in the well characterized samples. We also report superconductivity in a newly obtained compound BaNb$_2$Se$_5$ with BaTa$_2$S$_5$-type structure.

EXPERIMENTS

Samples with various compositions around BaNbSe$_3$ were prepared as follows. Mixtures of the desired ratios of Ba metal, Nb powder, and Se powder sealed in evacuated silica tubes (8 mm inner diameter) were gradually heated up to 800°C at a rate of 100°C/h and were annealed at this temperature for 5 days. To prevent the reaction of Ba metal with the silica tubes, the insides of the tubes were coated

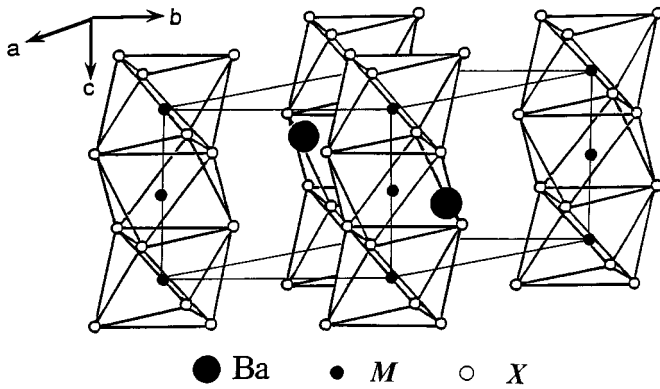[1] To whom correspondence should be addressed.

FIG. 1. Schematic drawing of the structure of BaMX_3 (M = Ti, V, Nb, Ta; X = S, Se) of a hexagonal BaVS$_3$-type structure with space group of $P6_3/mmc$.

with carbon film by means of pyrolysis of acetone, i.e., a small amount of acetone within the silica tube was burned in air using a strong flame, with the procedure being repeated several times. After grinding and pelletization, the products were sealed again in silica tubes and were sintered at 800°C for 5 days, followed by quenching to room temperature. X-ray powder diffraction measurements were performed at room temperature using a diffractometer RIGAKU RAD-B. The intensity data were collected with Cu$K\alpha$ radiation at 0.05° intervals. A RIETAN program was used for the Rietveld analysis (26). Differential scanning calorimetry (DSC) measurements were carried out from ~100 K to room temperature using MAC SCIENCE DSC-3100 with a heating–cooling rate of 10 K/min. Electrical resistivity ρ measurements were performed by an ordinary dc four-probe method from 2 to 273 K. Thermoelectric power (Seebeck coefficients S) measurements were made from ~100 K to room temperature using copper leads with a temperature gradient of ~0.3 K/cm, essentially as described previously (27). In both ρ and S measurements Cu leads were contacted with sintered pellets by gold paste. Magnetic susceptibility measurements were carried out using a SQUID magnetometer and a Faraday-type torsion balance.

RESULTS AND DISCUSSION

Structure and Single-Phase Region

Contrary to the earlier reports of preparations of stoichiometric compounds of BaMX_3 (13–15), Donohue and Weiher claimed that the compounds exist as a single phase in the nonstoichiometric composition of Ba$M_{0.8}X_3$ (M = Nb, Ta; X = S, Se), which formally requires d^0 pentavalent state of M, being consistent with the diamagnetic and the semiconductive behaviors (16). Chen $et\ al.$ also found that barium niobium triselenide is stable at the

composition BaNb$_{0.8}$Se$_3$ (18). Figure 2 (a) shows X-ray Rietveld refinements of BaNb$_{0.8}$Se$_3$. The calculated profile plots agree well with the observed patterns. Lattice parameters are a = 7.116(9) Å, c = 5.972(2) Å. The final R factors are R_{wp} = 5.7%, R_p = 4.4%, R_B = 9.2%, R_F = 5.8%, and R_e = 3.6%. Positional parameters and isotropic thermal parameters of three atoms are shown in Table 1. On the basis of the present results, the compound is considered to be stable at the composition of BaNb$_{0.8}$Se$_3$ rather than BaNbSe$_3$, which is consistent with the observations of Chen $et\ al.$ (18). Figure 2b shows X-ray Rietveld refinements of BaNb$_{0.95}$Se$_3$. The calculated profile plots agree well with the observed patterns. Lattice parameters are a = 7.117(7) Å and c = 5.969(1) Å and the final R factors are R_{wp} = 6.5%, R_p = 4.9%, R_B = 5.2%, R_F = 3.5%, and R_e = 3.7%. Positional parameters and isotropic thermal parameters of three atoms are shown in Table 1. Diffraction patterns of samples with Nb content more than 0.95 showed the coexistence with an impurity phase of BaNb$_2$Se$_5$. These observations show that the single-phase region extends from BaNb$_{0.8}$Se$_3$ to BaNb$_{0.95}$Se$_3$. For convenience, we refer to this phase as BaNbSe$_3$ phase.

Semiconductor-to-Metal (S–M) Transition

Figure 3 gives temperature variation of electrical resistivity ρ of BaNb$_{0.95}$Se$_3$. The ρ values increase with decreasing temperature down to ~140 K, indicative of semiconductive behavior; the energy gap was estimated to be Eg = 0.22 eV from the slope of logρ vs $1/T$ above 200 K. Upon further cooling, the ρ–T curve shows a cusp at ~140 K and then exhibits metallic behavior down to 2 K. The temperature dependence is similar to that observed in BaNbS$_3$ (23, 24). DSC measurements showed a small latent heat at the anomaly temperature, indicating that the anomaly is associated with a first-order phase transition. The transition will be referred to as semiconductor-to-metal (S–M) transition.

Figure 4 shows temperature variation of Seebeck coefficient S of BaNb$_{0.95}$Se$_3$. The value of S is ca. −180 μV/K at 300 K, indicating that the compound is a semiconductor. The value increases to ca. −20 μV/K at ~160 K as the temperature decreases. A small hysteresis was observed above ~200 K. The value of S below ~160 K seems to increase almost linearly as the temperature decreases. The temperature dependence as well as the rather small values of S show that the compound is a normal metal in this temperature region. These observations of S show that the transition is characterized by a change from semiconductive to metallic behavior, which is well consistent with the ρ measurements. The negative sign of S suggests that the dominant carriers are electrons. The electron conduction can be explained as follows on the basis of a band calculation presented by Whangbo $et\ al.$ for BaMS_3 (28). BaNb$_{0.80}$Se$_3$ has formal Nb^{5+} (d^0) ions, and thus there
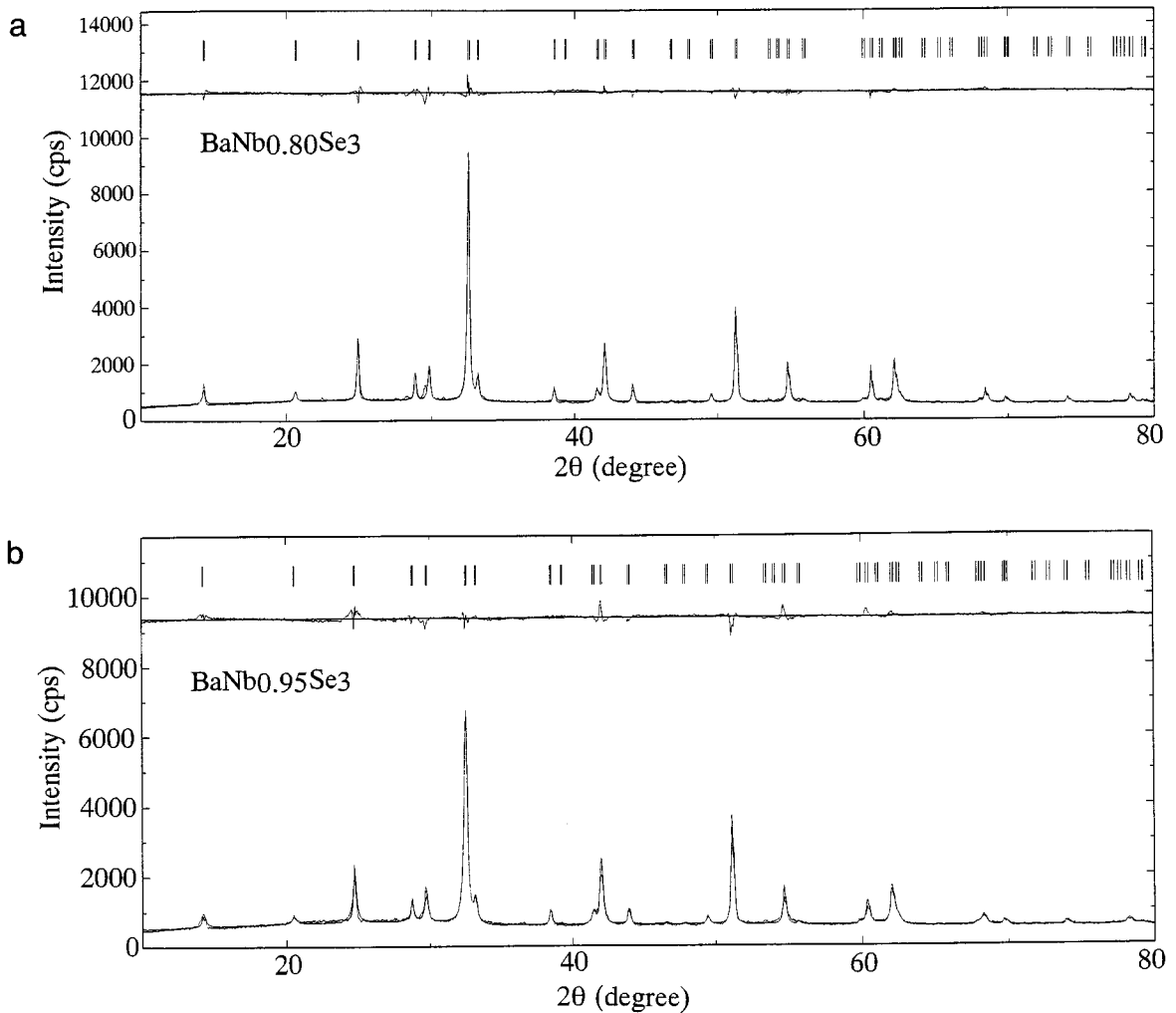
FIG. 2.   Profile fits of powder X-ray diffraction patterns obtained by Rietveld analysis of $BaNb_{0.80}Se_3$ (a) and $BaNb_{0.95}Se_3$ (b).

Table 1
Positional Parameters and Equivalent Isotropic Thermal Parameters of $BaNb_{0.80}Se_3$ and $BaNb_{0.95}Se_3$

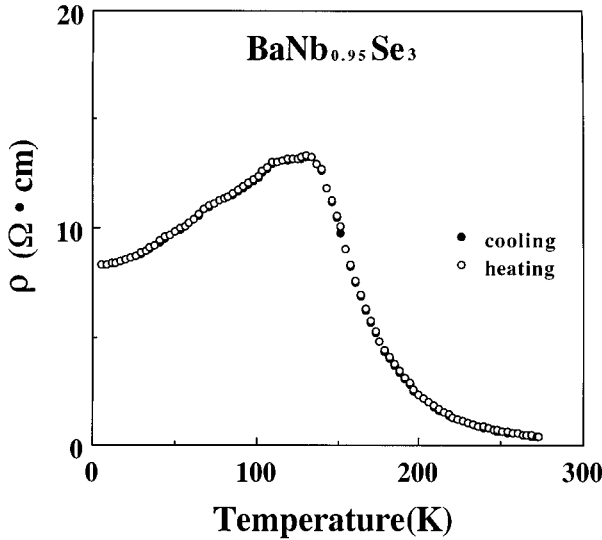| Atoms	x	y	z	U_{eq} (Å^2)[a]	occ.[b]
		$BaNb_{0.80}Se_3$			
Ba	1/3	2/3	3/4	0.27(3)	1.0
Nb	0	0	0	1.18(2)	0.80
Se	0.173(4)	0.345(1)	1/4	0.72(4)	1.0
		$BaNb_{0.95}Se_3$			
Ba	1/3	2/3	3/4	0.12(6)	1.0
Nb	0	0	0	2.04(2)	0.95
Se	0.175(1)	0.350(1)	1/4	0.14(5)	1.0

[a] $U_{eq} = (8\pi^2/3)\Sigma_i\Sigma_j U_{ij}a_i^* a_j^* \mathbf{a}_i \cdot \mathbf{a}_j$.
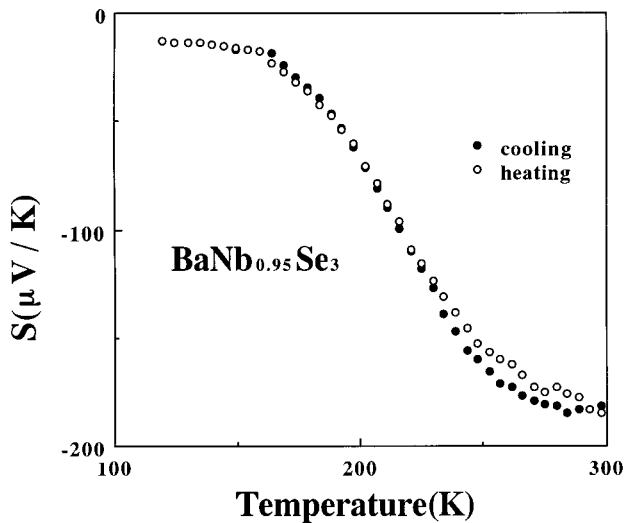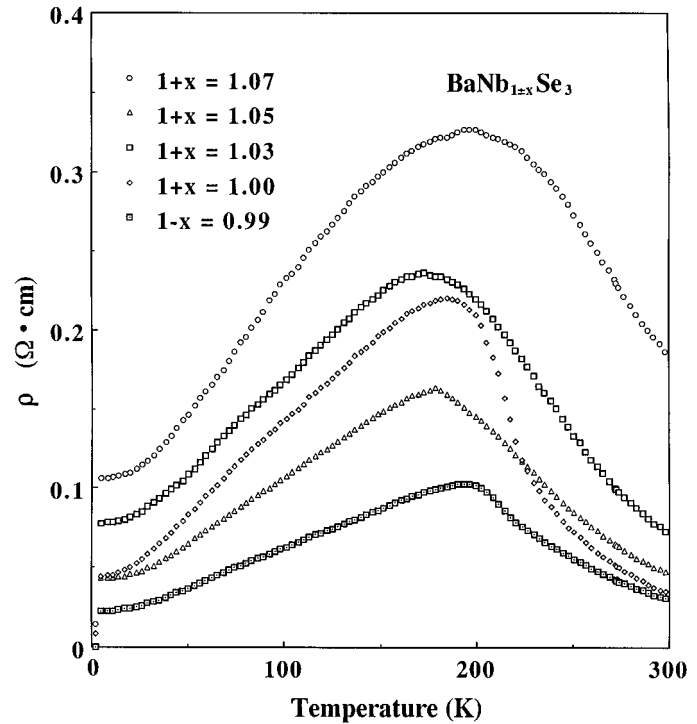[b] Site occupancy.

are no electrons in the d-block bands. Increasing the Nb content caused Nb^{4+} (d^1) ions to be introduced in the compound to maintain charge neutrality by supplying electrons to the d-block bands. Magnetic susceptibility χ measurements showed that $BaNb_{0.95}Se_3$ is diamagnetic. The value of χ is -7×10^{-8} emu/g at 300 K and slightly increases as the temperature decreases. The anomaly was not detected in χ measurements.

Figure 5 shows temperature variations of ρ of $BaNb_{1\pm x}Se_3$ ($0.99 \le 1 \pm x \le 1.07$). The samples show anomalies of ρ at ~ 200 K, which are similar to that of $BaNb_{0.95}Se_3$. X-ray diffraction measurements showed that the samples are in a two-phase mixing state consisting of $BaNb_{0.95}Se_3$ and a small amount of $BaNb_2Se_5$. $BaNb_2Se_5$ shows no transition down to 2.5 K, as described below. Accordingly, these anomalies can be assigned to be the S–M

FIG. 3. Temperature variation of electrical resistivity ρ of BaNb$_{0.95}$Se$_3$.

FIG. 5. Temperature variations of electrical resistivity ρ of BaNb$_{1 \pm x}$Se$_3$ ($0.99 \leq 1 \pm x \leq 1.07$). For simplicity, only the results on cooling are shown.

transition, which is intrinsic to BaNb$_{0.95}$Se$_3$. The values of ρ are lower than those of BaNb$_{0.95}$Se$_3$, which may be due to the coexistence of metallic impurity phase of BaNb$_2$Se$_5$. The coexistence of BaNb$_2$Se$_5$ phase was able to be easily detected by the observation of a superconductivity originating from the BaNb$_2$Se$_5$ phase. The details will be described below. Another notable result for these samples is that the compounds exhibit a small shoulder-like anomaly at ~ 70 K as shown in Figs. 3 and 5, indicative of the existence of another transition. The samples with Nb content of less than 0.95, BaNb$_{1-x}$Se$_3$ ($0.80 \leq 1 - x < 0.95$), showed semiconductive behaviors with the energy gap,

$E_g \approx 0.3$ eV. The S–M transition immediately disappears when the Nb content becomes only slightly smaller than 0.95. The superconductivity appears when the Nb content becomes only slightly larger than 0.95, indicative of the coexistence of BaNb$_2$Se$_5$ phase. Accordingly, the compositions exhibiting the S–M transition are considered to be restricted to a very narrow composition range around BaNb$_{0.95}$Se$_3$.

Figure 6 gives temperature variations of Seebeck coefficients S of BaNb$_{1 \pm x}$Se$_3$ ($0.99 \leq 1 \pm x \leq 1.07$). The change from semiconductive to metallic behavior was observed in all samples, which is similar to BaNb$_{0.95}$Se$_3$. The values of S above the transition are smaller than those of BaNb$_{0.95}$Se$_3$, which are considered to be due to the contamination of the metallic BaNb$_2$Se$_5$ phase.

Since the carrier concentration is considered to increase with increasing the Nb content in BaNb$_{1-x}$Se$_3$ ($0.80 \leq 1 - x < 0.95$), the appearance of the S–M transition in BaNb$_{0.95}$Se$_3$ may be correlated with the rather large number of conduction electrons. The Mott transition caused by a strong electron correlation, therefore, may be a candidate for the transition. Similar transition from a semiconductor to a metal on cooling was observed in the Ni(S$_{1-x}$Se$_x$)$_2$ system (29). Another possibility is that the transition is of a CDW-type which originates from the electron–phonon
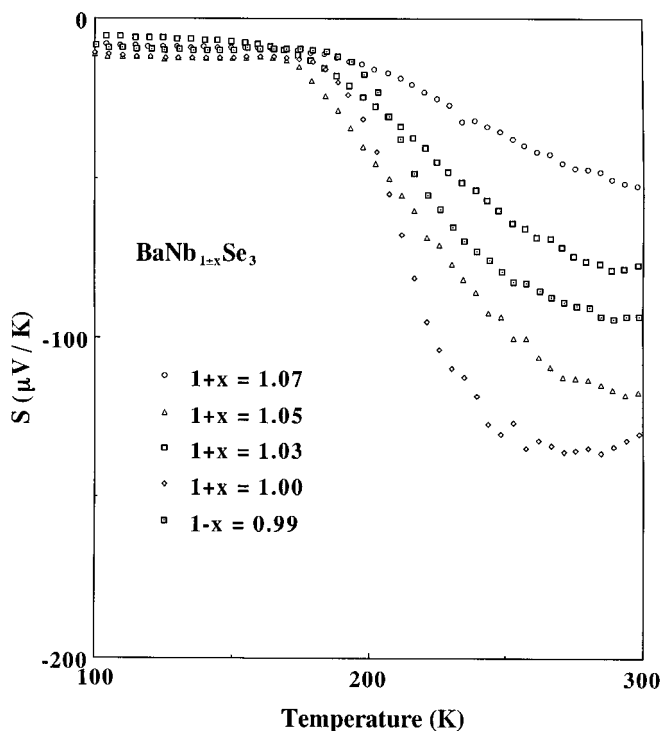

FIG. 4. Temperature variation of Seebeck coefficients S of BaNb$_{0.95}$Se$_3$.

FIG. 6. Temperature variations of Seebeck coefficients S of $BaNb_{1 \pm x}$ Se_3 ($0.99 \leq 1 \pm x \leq 1.07$). The results on cooling are shown.

interaction. $Ti_{1+x}Se_2$ shows such a temperature dependence of ρ (30). However, this possibility cannot explain the metallic conduction below the transition. Band calculations as well as structural investigations are needed to reveal the origin of the transition.

Semiconductor-to-semiconductor (S–S) Transition

Figure 7 gives temperature dependences of ρ of Ba_{1+x} $NbSe_3$ ($1.03 \leq 1 + x \leq 1.10$). All samples contain a small amount of an unknown impurity phase. Samples of $1 + x = 1.07$ and 1.10 show semiconductive behavior in all measured temperature ranges. The energy gap for each sample is $Eg = 0.32$ eV. On the other hand, samples with $1 + x = 1.03$ and 1.05, respectively, show an obvious anomaly at ~ 250 K and at ~ 200 K. Each anomaly is characterized by a jump in ρ with decreasing temperature, suggesting the presence of a phase transition, which will be referred to as semiconductor-to-semiconductor (S–S) transition. The values of energy gap below and above the transition for both compounds are ~ 0.3 eV.

Temperature variations of the Seebeck coefficients S for $Ba_{1+x}NbSe_3$ ($1.03 \leq 1 + x \leq 1.10$) are shown in Fig. 8. The S values at 300 K for the semiconducting samples of $1 + x = 1.07$ and 1.10 are ca. -0.25 mV/K and decrease
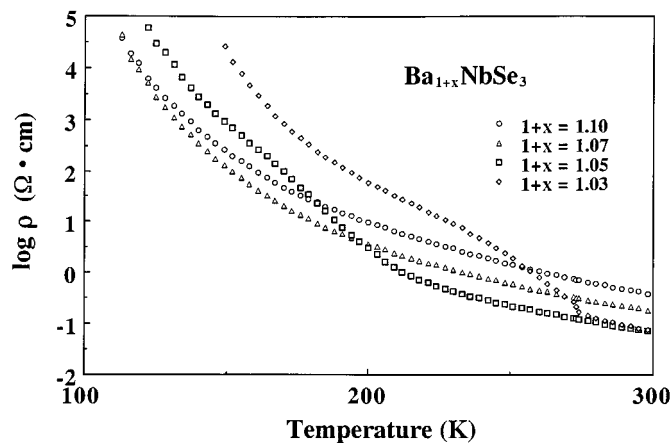

FIG. 7. Temperature variations of electrical resistivity ρ for Ba_{1+x} $NbSe_3$ ($1.03 \leq 1 + x \leq 1.10$). The results on cooling are shown.

with decreasing temperature down to ca. -2 mV/K. The large values are consistent with the semiconductive behaviors observed in ρ measurements. The S–S transition is more definitely observed in the S–T curves in the samples of $1 + x = 1.03$ and 1.05, where the S values gradually decrease with decreasing temperature and change sign from minus to plus near the transition. The large S values indicate that the compounds are semiconductors both above and below the transition. The change of the sign suggests that the dominant carriers change from electrons to holes at the transition. No latent heat was detected in DSC measurements at the S–S transition, whereas hysteresis was observed above the transition in both ρ and S measurements, indicating that the transition is of the first order, which may
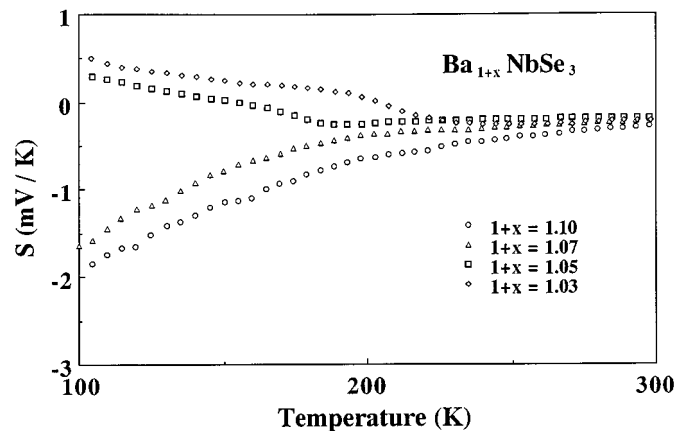

FIG. 8. Temperature variations of Seebeck coefficients S for Ba_{1+x} $NbSe_3$ ($1.03 \leq 1 + x \leq 1.10$). The results on cooling are shown.

be responsible for the drastic change of the conduction carriers. These samples showed a small values of χ of $\sim 10^{-8}$ emu/g at 300 K and showed a tendency of gradual increase with decreasing temperature. No anomaly was detected in the χ measurements.

Occurrences of S–M and S–S Transitions

Figure 9a shows partial ternary diagram of the Ba–Nb–Se system, indicating the relative positions of $BaNbSe_3$, $BaNb_{0.80}Se_3$, and $BaNb_2Se_5$. Figure 9b gives a more detailed diagram around the composition of $BaNbSe_3$. Figure 9b corresponds to the small triangle inside the diagram of Fig. 9a. Closed circles, open squares, open circles, and closed squares designate, respectively, the samples exhibiting the S–M transition, the S–S transition, metallic behavior, and semiconductive behavior. $BaNb_{0.95}Se_3$ is shown as the closed circle situated at the extreme right on the $BaNb_{1\pm x}Se_3$ line. The samples exhibiting the S–M transition correspond to $Ba_{1-\delta}Nb_{1\pm x}Se_3$ $(0.9 < 1 - \delta < 1.0, 0.95 < 1 \pm x < 1.10)$. These samples except for the single phase sample of $BaNb_{0.95}Se_3$ contain the $BaNbSe_3$ phase and a small amount of the $BaNb_2Se_5$ phase. On the basis of the same discussion as adopted for the $BaNb_{1\pm x}Se_3$ system, the observed S–M transitions are considered to be intrinsic to $BaNb_{0.95}Se_3$, which is located at the Nb-rich boundary of the single-phase region of the $BaNbSe_3$ phase. It is most likely that the transition is intrinsic to the slightly Ba-deficient $BaNb_{0.95}Se_3$ sample, because the compositions

exhibiting the S–M transition lie in the Ba-poor region. However, the Ba deficiency was too small to be determined precisely. All samples exhibiting the S–M transition except for $BaNb_{0.95}Se_3$ showed a superconductivity at 2.5 K. SQUID measurements of these samples showed that the diamagnetic values below 2.5 K increase as the composition approaches the $BaNb_2Se_5$, which implies that the superconductivity originates from the $BaNb_2Se_5$ phase. The superconductivity of $BaNb_2Se_5$ will be discussed in more detail below.

The S–S transition was observed in many Ba-rich samples with compositions of $Ba_{1+\delta}Nb_{1\pm x}Se_3$ $(1.0 < 1 + \delta < 1.13, 0.97 < 1 \pm x < 1.07)$, which are shown in Fig. 9b as open squares. All samples exhibiting the S–S transition contain a small amount of unknown impurity phase. It seems possible that the impurity phase is responsible for the transition. This possibility, however, may be excluded because the transition was not observed in samples situated far from the single-phase region as shown by closed squares, which contain the larger amount of the impurity phase. The S–S transition is possibly intrinsic to the very slightly Ba-rich $BaNb_{0.95}Se_3$ sample, because samples exhibiting the S–S transition lie in the Ba-rich region.

Superconductivity of a New Phase of $BaNb_2Se_5$

The X-ray diffraction pattern of $BaNb_2Se_5$ showed a $BaTa_2S_5$-type structure which has a complex superstructure with hexagonal subcell of $a = 3.326$ Å and $c = 25.21$ Å (31),
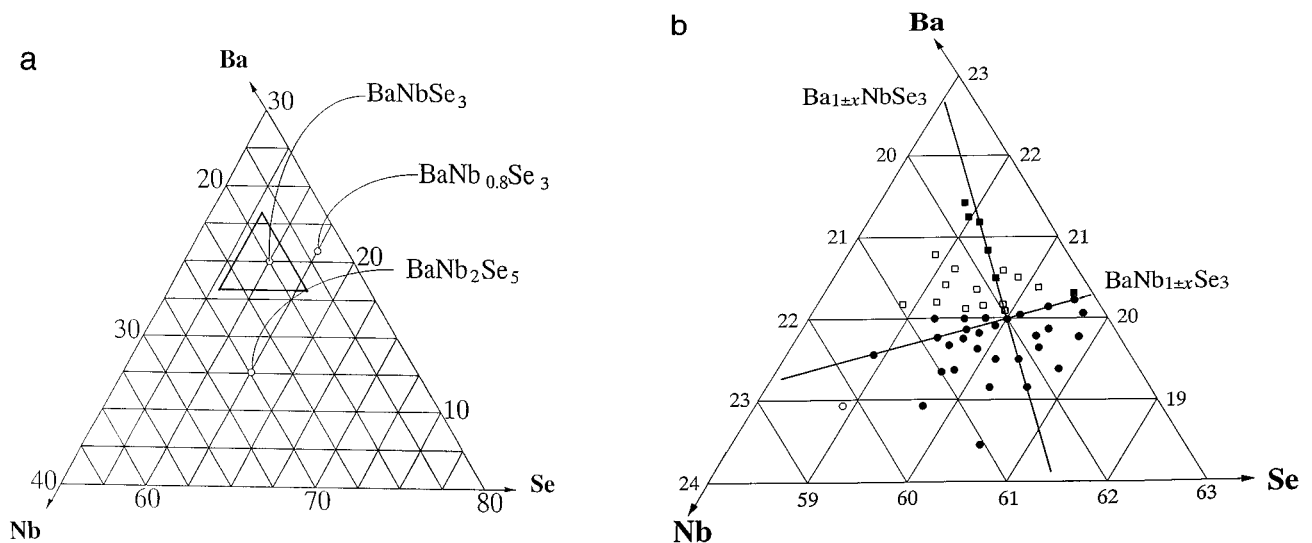

FIG. 9. (a) Partial ternary diagram of Ba–Nb–Se system indicating relative positions of $BaNbSe_3$, $BaNb_{0.80}Se_3$, and $BaNb_2Se_5$. The scales are mole percents. (b) Partial ternary diagram of Ba–Nb–Se system around the composition of $BaNbSe_3$. The diagram corresponds to the small triangle inside the partial diagram of (a). Samples were obtained by quenching from 800°C. Closed circles, open squares, open circles, and closed squares designate, respectively, the samples exhibiting the S–M transition, the S–S transition, metallic behavior, and semiconductive behavior. The closed circle at the extreme right on the $BaNb_{1\pm x}Se_3$ line shows $BaNb_{0.95}Se_3$. The intersecting point of the straight lines of $BaNb_{1\pm x}Se_3$ and $Ba_{1\pm x}NbSe_3$ corresponds to the composition $BaNbSe_3$.
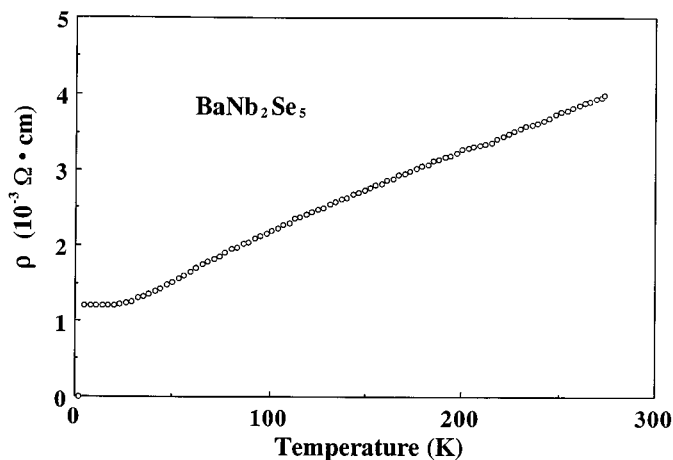
FIG. 10. Temperature variation of electrical resistivity ρ of BaNb$_2$Se$_5$ measured on cooling.

although several small unknown peaks were found. The lattice parameters of BaNb$_2$Se$_5$ were calculated to be $a = 3.4501$ Å and $c = 25.795$ Å. Although the precise structure of BaTa$_2$S$_5$ has not yet been determined, BaNb$_2$Se$_5$ is considered to have a layered-type structure because of the X-ray pattern exhibiting preferred orientation in 001 planes, which is also the case in BaTa$_2$S$_5$ (31). Figure 10 gives the temperature dependence of ρ of BaNb$_2$Se$_5$. The compound shows metallic behavior, with the values of ρ being on the order of 10^{-3} $\Omega \cdot$ cm. Superconductivity was observed at ~ 2.5 K. The superconductivity was confirmed by magnetic susceptibility χ measurements as shown in Fig. 11. The value of χ in the superconducting state is expected to be ca. -10^{-2} emu/g, assuming that the bulk of the sample is a pure superconductor. The present value of χ of -1.14×10^{-3} emu/g at 2 K can be sufficiently large for considering that the compound is a superconductor. The present results are similar to those of BaTa$_2$S$_5$ which shows superconductivity at ~ 3 K (32).
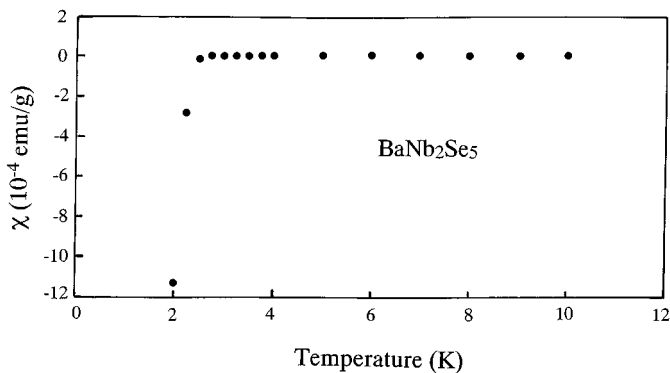
CONCLUSIONS

Quasi-one-dimensional compound BaNbSe$_3$ was found to be stable in the composition range BaNb$_{1-x}$Se$_3$ ($0.80 \leq 1 - x \leq 0.95$). BaNb$_{0.95}Se_3$ showed a first-order semiconductor-to-metal (S–M) transition at ~ 140 K. The detailed phase study revealed that the transition seems to be intrinsic to the sample of slightly Ba-deficient BaNb$_{0.95}$Se$_3$. The S–M transition was also observed in Seebeck measurements. The dominant carriers were found to be electrons above and below the transition, which may originate from Nb^{4+} (d^1) ions. A semiconductor-to-semiconductor (S–S) transition was observed in slightly Ba-rich BaNb$_{0.95}$Se$_3$. The transition is characterized by a jump of ρ on cooling at 200–300 K. The sign of Seebeck coefficient changes from negative to positive, indicating a drastic change of the band structure. Structural investigations at low temperatures are needed to clarify the origins of both transitions. Superconductivity was observed at 2.5 K in a newly obtained BaNb$_2$Se$_5$ with the BaTa$_2$S$_5$-type structure.

FIG. 11. Temperature variation of magnetic susceptibility χ of BaNb$_2$Se$_5$ measured on cooling.

REFERENCES

1. L. P. Gor'kov and G. Grüner, "Charge Density Waves in Solids," North-Holland, Amsterdam, 1989.
2. A. Meerschaut and J. Rouxel, in "Crystal Chemistry and Properties of Materials with Quasi-one-dimensional Structure" (J. Rouxel, Ed.), p. 205. Reidel, Dordrecht, 1986.
3. Z. Z. Wang, P. Monceau, M. Renard, P. Gressier, L. Guemas, and A. Meerschaut, *Solid State Commun.* **47,** 439 (1983).
4. Y. Ishihara and I. Nakada, *Solid State Commun.* **42,** 579 (1982); **44,** 1439 (1982).
5. T. Sekine, Y. Kiuchi, E. Matsuura, K. Uchinokura, and R. Yoshizaki, *Phys. Rev. B* **36,** 3153 (1987).
6. T. Ohtani, Y. Sano, and Y. Yokota, *J. Solid State Chem.* **103,** 504 (1993).
7. J.-G. Lee, S. Chan, K. V. Ramanujachary, and M. Greenblatt, *J. Solid State Chem.* **121,** 332 (1996).
8. T. Ohtani, J. Ogura, M. Sakai, and Y. Sano, *Solid State Commun.* **78,** 913 (1991).
9. T. Ohtani, J. Ogura, H. Yoshihara, and Y. Yokota, *J. Solid State Chem.* **115,** 379 (1995).
10. L. W. ter Haar, F. J. DiSalvo, H. E. Bair, T. M. Fleming, J. V. Waszczak, and W. E. Hatfield, *Phys. Rev. B* **35,** 1932 (1987).
11. R. M. Fleming, L. W. ter Haar, and F. J. DiSalvo, *Phys. Rev. B* **35,** 5388 (1987).
12. H. Sato, N. Kojima, K. Suzuki, and T. Enoki, *J. Phys. Soc. Jpn.* **62,** 647 (1993).
13. L. A. Aslanov and M. Kovba, *Zh. Neorg. Khim.* **9,** 2441 (1964); *Russ. J. Inorg. Chem.* **9,** 1317 (1964).

14. R. A. Gardner, M. Vlasse, and A. Wold, *Inorg. Chem.* **8,** 2784 (1969).
15. R. A. Gardner, M. Blasse, and A. Wold, *Acta Crystallogr. B* **25,** 781 (1969).
16. P. C. Donohue and J. F. Weiher, *J. Solid State Chem.* **10,** 142 (1974).
17. P. C. Donohue, *Mater. Res. Bull.* **10,** 57 (1975).
18. B.-H. Chen, G. Sàghi-Szabó, B. Eichhorn, J.-L. Peng, and R. Greene, *Mater. Res. Bull.* **27,** 1249 (1992).
19. M. Takano, H. Kosugi, N. Nakanishi, M. Shimada, T. Wada, and M. Koizumi, *J. Phys. Soc. Jpn.* **43,** 1101 (1977).
20. H. Nishihara and M. Takano, *J. Phys. Soc. Jpn.* **50,** 426 (1981).
21. O. Massenet, R. Buder, J. J. Since, C. Schlenker, J. Mercier, J. Kelber, and D. G. Stucky, *Mater. Res. Bull.* **13,** 187 (1978).
22. M. Nakamura, A. Sekiyama, H. Namatame, A. Fujimori, H. Yoshihara, T. Ohtani, A. Misu, and M. Takano, *Phys. Rev. B* **49,** 16191 (1994).
23. J. Yan, K. V. Ramanujachary, and M. Greenblatt, *Mater. Res. Bull.* **30,** 463 (1995).
24. S.-J. Kim, H.-S. Bae, K.-A. Yee, J.-H. Choy, D.-K. Kim, and N.-H. Hur, *J. Solid State Chem.* **115,** 427 (1995).
25. T. Ohtani, "Annual Report of Science Research on Priority Area, Ministry of Education, Science and Culture," Japan, p. 94. 1994. [in Japanese, unpublished]
26. F. Izumi, *Nippon Kessho Gakkaishi* **27,** 23 (1985). [in Japanese]; F. Izumi, *in* "The Rietveld Method" (R. A. Young, Ed.), p. 236. Oxford Univ. Press, New York, 1993.
27. T. Ohtani, *J. Phys. Soc. Jpn.* **37,** 701 (1974).
28. M.-H. Whangbo, M. J. Foshee, and R. Hoffmann, *Inorg. Chem.* **19,** 1723 (1980).
29. P. Kwizera, M.S. Dresselhaus, and D. Adler, *Phys. Rev. B* **21,** 2328 (1980).
30. F. J. DiSalvo, D. E. Moncton, and J. V. Waszczak, *Phys. Rev. B* **14,** 4321 (1976).
31. M. Saeki, H. Nozaki, and M. Onoda, *Mater. Res. Bull.* **24,** 851 (1989).
32. H. Nozaki, M. Saeki, and M. Onoda, *J. Solid State Chem.* **116,** 392 (1995).